

Received September 21, 2020; reviewed; accepted November 17, 2020

Study on surface modification of cerussite by thermochemical processing with pyrite

Yong-Xing Zheng^{1,3}, Ji-Lai Ning¹, Hai-Yun Xie^{1,2}, Jin-Fang Lv², Pan-Jin Hu¹, Jie Pang²

¹ State Key Laboratory of Complex Nonferrous Metal Resources Clean Utilization, Kunming University of Science and Technology, Kunming 650093, China

² Faculty of Land Resource Engineering, Kunming University of Science and Technology, Kunming 650093, China

³ Faculty of Metallurgical and Energy Engineering, Kunming University of Science and Technology, Kunming 650093, China

Corresponding authors: xiehaiyunkm@163.com (Hai-Yun Xie), jflv2017@126.com (Jin-Fang Lv)

Abstract: In this paper, surface modification of cerussite by thermochemical processing with pyrite was studied based on microflotation tests, X-ray powder diffractometry (XRD), X-ray photoelectron spectroscopy (XPS) and electron probe microanalysis (EPMA). Microflotation test results showed that the surface modification facilitated flotation of the treated cerussite and improved the flotation recovery to approximately 90%. The results of XRD analyses confirmed that cerussite was transformed into massicot, which then interacted with pyrite to form PbS, PbSO₄, PbO·PbSO₄ and 4PbO·PbSO₄. XPS analyses results revealed that both PbS and PbS₂ were formed on the mineral surface, and the percentage of PbS increased with increasing FeS₂/PbCO₃ (F/P) mole ratio, which was advantageous for the flotation of the modified cerussite. EPMA analyses showed that particles with layered configurations were obviously formed after thermochemical processing. The thickness of the products at the outer layer of the particles increased when the F/P mole ratio increased. Moreover, the S and O contents in the products increased and decreased, respectively.

Keywords: cerussite, pyrite, surface modification, thermochemical processing, flotation

1. Introduction

Lead is widely used in various industries, such as batteries, machinery manufacturing and optical components (Ivanov et al., 2000; Korshin et al., 2000; Sharonov et al., 2008; May et al., 2018). Lead is usually extracted from lead sulfide and lead oxide minerals. Galena (PbS) is a representative natural lead sulfide mineral and has mainly been used as a raw material for lead production in the past few years. With the depletion of sulfide mineral resources, oxide mineral resources are being exploited. Cerussite (PbCO₃), as a typical lead oxide mineral, mainly exists in oxide ore, and there are considerable amounts of lead oxide ore in China (Tang et al., 2014; Wang et al., 2014). Flotation has been the most commonly applied method for concentrating the cerussite.

Cerussite is a kind of semi-soluble salt mineral with a high solubility constant (Shirota et al., 2011; Powell et al., 2013). When xanthate is directly added to float cerussite, the lead ions from the mineral lattice are initially dissolved and then enter the pulp solution. Then, the lead ions interact with the added xanthate to form a lead xanthate precipitate in the bulk solution and at the surface of the cerussite (Fuerstenau et al., 1987; Herrera-Urbina et al., 1998). The former situation not only has little effect on the surface hydrophobicity of the mineral, but also consumes large amounts of xanthate. The latter situation can make the surface of the cerussite hydrophobic. However, lead xanthate is only weakly linked to the surface. It is well known that nonferrous sulfide minerals are more easily floated than their corresponding oxide minerals. If an effective method was developed to transform the surface of the cerussite, even the whole cerussite, into the lead sulfide mineral, the obtained cerussite could be effectively floated with conventional collectors. Sodium sulfide (Na₂S) and sodium hydrogen sulfide

(NaHS) are usually used to convert the surface of the cerussite into lead sulfide (Malghan, 1986; Gush, 2005). Employing higher or lower amounts of sulfidation agent is not conducive to flotation of the cerussite. In other words, accurately adding the sulfidation agent is a difficult task. Moreover, the sulfide film formed on the surface easily detaches during the flotation process.

Recently, multiple methods, including mechanochemical processing (Yuan et al., 2012; Li et al., 2017), hydrothermal treatment (Li et al., 2012; Liang et al., 2012) and sulfidation roasting (Li et al., 2010; Zheng et al., 2015; Chen et al., 2019), have been reported for improving the sulfidation performance. Li et al. (2017) and Yuan et al. (2012) adopted a method of co-grinding lead oxide with sulfur under mild conditions prior to flotation. The results showed that the floatability of lead oxide cannot be satisfactory attributed to the disproportionation reactions of sulfur, resulting in the formation of $PbSO_4$ and PbS . Liang et al. (2012) and Li et al. (2012) reported the hydrothermal sulfidation of lead-containing materials and their flotation performance. It was confirmed that the sulfurized lead oxide minerals floated well. However, the whole sulfidation process had to be performed in an airtight environment. In addition, the process required a long reaction time to obtain a high sulfidation extent. Sulfidation roasting may be promising for improving the reaction rate and the continuous production. Li et al. (2010) reported the sulfidation roasting of a low-grade lead-zinc oxide ore with sulfur in an airtight device. The results showed that the sulfidation ratio of lead oxide increased to 98%, and the flotation recovery of lead reached 79.5%. Zheng et al. (2015) found that sulfidation roasting could be carried out in an incompletely sealed environment by optimizing the reaction process. In addition, it was confirmed that only surface modification can facilitate the flotation of cerussite. After surface sulfidation a Pb-Zn oxide ore with sulfur at a high temperature, the lead recovery reached 92.3% after a closed-circuit flotation test (Chen et al., 2019).

Generally, the floatability of the cerussite significantly improved after thermochemical processing. Pyrite and sulfur are two commonly used sulfidation agents. Pyrite can slowly release sulfur vapor from its crystal lattice, which made the sulfidation process be more readily controlled in contrast with sulfur (Zheng et al., 2018a; Zheng et al., 2018b). The reported literature mainly focused on the synthesis and thermal decomposition of pyrite (Golsheikh et al., 2013; Lv et al., 2015). Our team further investigated the interaction mechanism between pyrite and the decomposed cerussite at high temperatures, mainly focusing on the evolution process and the characteristics of crystal growth (Zheng et al., 2018a). However, there is a lack of information about the changes to the surface of the cerussite caused by thermochemical processing. Moreover, the floatability of oxide minerals usually greatly depends on the surface sulfidation performance. Therefore, it is essential to deeply investigate the surface modification mechanism of cerussite in the presence of pyrite.

In this study, microflotation tests, X-ray powder diffractometry (XRD), X-ray photoelectron spectroscopy (XPS) and electron probe microanalysis-energy dispersion spectrum (EPMA-EDS) were conducted to investigate the interaction mechanism between the cerussite and pyrite under thermochemical conditions and to further improve the sulfidation performance of the cerussite.

2. Experimental

2.1. Materials and reagents

A crude cerussite sample was provided from a mine in Yunnan Province, China, and was followed by artificial removal of gangue such as quartz, hematite and calcite. The purified cerussite sample was dry ground in an agate mortar and then sieved to obtain a particle size range from -74 to $37 \mu\text{m}$ for thermochemical processing and various tests. The XRD pattern of the obtained cerussite sample is shown in Fig. 1, which revealed that there were nearly no impurities in the sample. Pyrite was used as the sulfidation agent in the thermochemical processing. The XRD pattern of pyrite is shown in Fig. 2, which indicates that the sample also had few impurities. Nitrogen (99.99%) was used as a protective gas.

Sodium hydroxide (NaOH) and hydrochloric acid (HCl) were used to adjust the pulp pH in the flotation experiments. Ethyl xanthate was used as the collector, and terpineol was used as the frother.

2.2. Thermochemical processing and microflotation tests

The pyrite was initially mixed with the prepared cerussite, and the mixed sample was placed into a 50

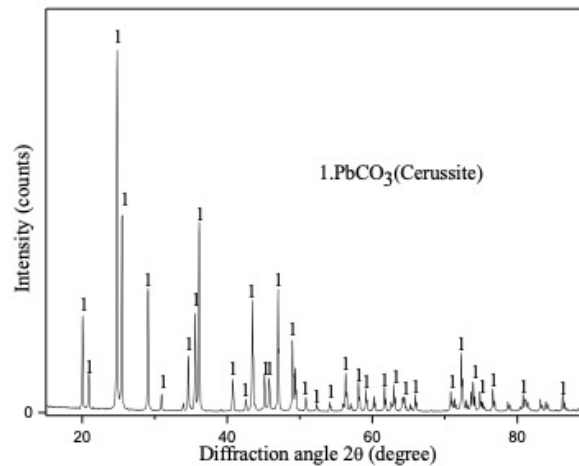


Fig. 1. XRD pattern of the cerussite

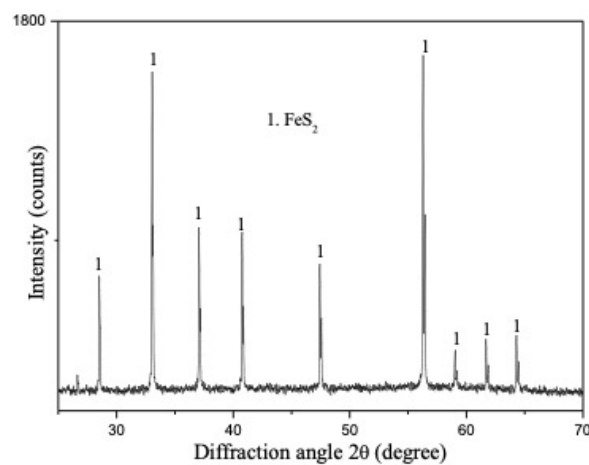


Fig. 2. XRD pattern of the pyrite

mL glass tube. The tube was slowly pushed into a corundum tube, while nitrogen was inlet as an inert gas with a velocity of 1.0 L/min. The whole equipment was heated at a heating rate of 10°C/min. As soon as the desired temperature was reached, the mixed sample was kept at the temperature for 60 min. After thermochemical processing, the obtained sample was cooled in the presence of nitrogen. Our previous studies confirmed that lead oxide was well sulfurized in a temperature range of 450°C to 650°C (Zheng et al., 2015; Zheng et al., 2018a; Chen et al., 2019). Therefore, a moderate temperature of 600°C was selected in this study.

Approximately 2 g of the obtained sample was placed in a microflotation cell (40 mL), and then 35 mL of distilled water was added. The pulp pH was adjusted, followed by the addition of ethyl xanthate and terpineol. After 2 min of flotation time, the concentrate and tailing were washed with distilled water, filtered and dried.

2.3. XRD analyses

The phase changes for the cerussite before and after interacting with pyrite were identified making use of a Germany Bruker-axs D8 Advance X-ray powder diffractometer (XRD) with K α radiation ($\lambda=1.5406$ Å). The obtained data were analyzed by a software (MDI Jade 6) of XRD pattern processing and identification.

2.4. XPS analyses

XPS is a significantly forceful tool for investigating chemical constituents and chemical states of element at the surface. The obtained sample was determined in a Thermo Fisher Scientific equipment with a

resolution of 0.2 eV, a working pressure lower than 2×10^{-7} mbar and Al K α monochromatic irradiation. A survey scan of the obtained sample was conducted to detect elemental information. Then, the Thermo Avantage software was used for fitting XPS spectrums of specific elements, such as S, O, Pb, Fe and C. The spectrometer was calibrated by fixing binding energy of C 1s at 284.8 eV.

2.5. EPMA-EDS analyses

The modified cerussite samples were mounted in an epoxy resin and carefully polished. The carbon powder was sprayed at the surface of the polished sample prior to EPMA-EDS analysis due to its poor conductivity. Then, EPMA-EDS analysis was carried out to investigate the surface morphology and constituents of the cerussite before and after the thermochemical proceeding with pyrite. Probe current was set to 20 nm and acceleration voltage was set to 20 kV.

3. Results and discussion

3.1 Microflotation tests of the cerussite after surface modification

The effects of ethyl xanthate dosage and pH on the floatability of cerussite after modification with different F/P mole ratios are shown in Fig. 3. As shown in Fig. 3(a), the ethyl xanthate had a stronger flotation capability towards the modified cerussite. A satisfactory F/P mole ratio was 0.3 or 0.4. At an F/P mole ratio of 0.4, the ethyl xanthate floated out 90% of the modified cerussite when the collector dosage was fixed as 10×10^{-5} . However, ethyl xanthate at the same dosage only floated out 15% of the cerussite modified with an F/P mole ratio of 0.1. It was obvious that the recovery of the modified cerussite increased with the increase in the F/P mole ratio.

As presented in Fig. 3(b), the flotation recovery of the cerussite modified with the same F/P mole ratio was slightly affected by the pH in the range of 3-9. When the pH was above 9.0, the flotation recovery of the modified cerussite intensively decreased. However, the F/P mole ratios greatly affected the flotation recovery of the modified cerussite. The results indicated that flotation of the modified cerussite required not only selecting an appropriate F/P mole ratio, but also screening for the optimum flotation pH.

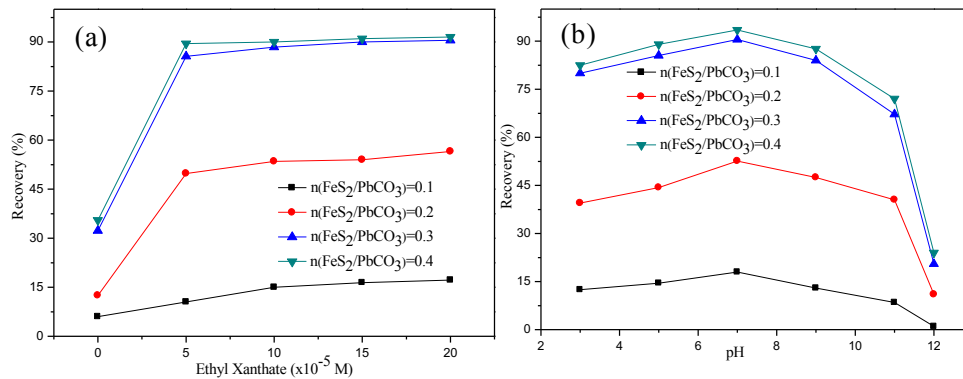


Fig. 3. Flotation recovery of the modified cerussite as functions of (a) collector dosage (pH = 7.0) and (b) pH (ethyl xanthate dosage of 10×10^{-5} M)

3.2 XRD analyses

Fig. 4 shows the XRD patterns of the cerussite after thermochemical processing with different F/P mole ratios. According to this figure, the cerussite completely disappeared (Eq. (1)), while Pb-bearing species, such as PbS, Pb₂(SO₄)O, Pb₅O₄SO₄ and PbO, were formed with the introduction of pyrite at an F/P mole ratio of 0.1. With a further increase in the F/P mole ratio, the peak intensity of PbS increased. However, the peak intensities of Pb₂(SO₄)O and Pb₅O₄SO₄ decreased and even disappeared. Therefore, the increase in the F/P mole ratio was advantageous to the generation of PbS.

To investigate the thermochemical reaction mechanism of the cerussite and pyrite, their equilibrium phase composition was calculated by the equilibrium composition module of Outokumpu HSC 6.0 (Roine, 2002). The calculations were conducted for 1 kmol of PbCO₃ at 600°C at 1 atm, and the results

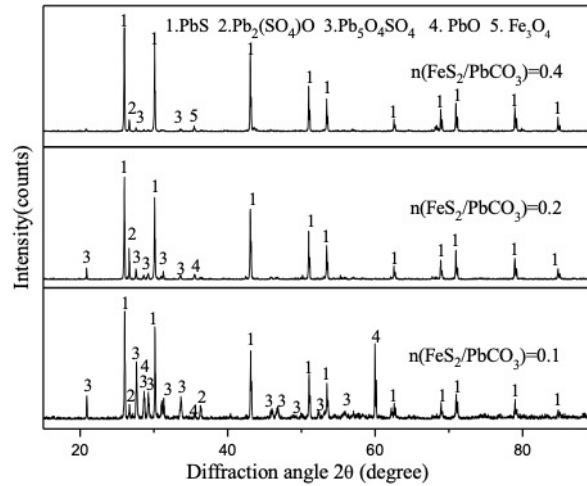


Fig. 4. XRD patterns of the cerussite modified with different F/P mole ratios

are shown in Fig. 5. From Fig. 5(a), the generated PbO was completely transformed into PbS (Eqs. 2-3) when the amount of pyrite was fixed at 0.6 kmol, which corresponds to an F/P mole ratio of 0.6. When the amount of pyrite was below 0.6 kmol, the generated PbO interacted with the pyrite or sulfur vapor originating from the decomposition of pyrite, forming PbS, PbSO₄ (Eqs. (3, 4)) and PbSO₄-bearing intermediates (Eqs. (5, 6)), such as PbO·PbSO₄ and 4PbO·PbSO₄, as shown in the expanded view (Fig. 5(b)), which agreed with the results obtained in Fig. 4. According to Fig. 3, the recovery of the treated cerussite reached 90% when the F/P mole ratio was fixed at 0.3 or 0.4. Both values were below the theoretical F/P mole ratio (0.6) for thoroughly transforming PbCO₃ into PbS, which indicated that only the outer layer of the lead oxide mineral was transformed into PbS.

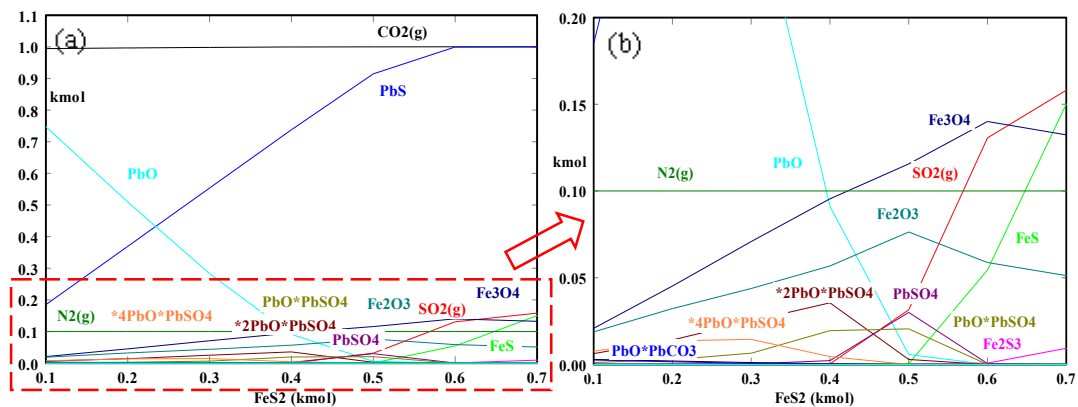
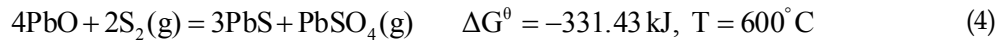
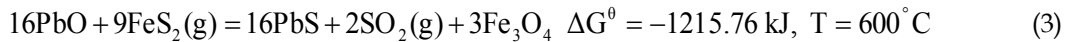
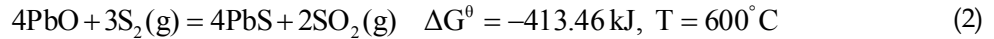


Fig. 5. Equilibrium composition of the cerussite after thermochemical processing as a function of pyrite dosage (1 kmol PbCO₃, 600°C, 1 atm)

3.3. XPS analyses

Fig. 6 shows the full range XPS spectra of the cerussite before and after thermochemical processing with pyrite. According to the XPS pattern, the key elements, such as Pb, S, O and C showed strong signals.

In addition, the peak intensity of S and O increased and decreased, respectively, with the increase in the F/P mole ratio. Table 1 lists the surface concentrations of Pb, S, O, C and Fe atoms. From this table, the concentrations of Pb, Fe, O, C and S atoms on the surface of the untreated cerussite were 13.33%, 0.61%, 49.64%, 36.42% and 0%, respectively. After thermochemical processing of the sample with a lower F/P mole ratio (Sample B), the concentrations of Pb, Fe and S atoms increased, whereas the concentration of O atoms decreased. This result can be attributed to the decomposition of PbCO_3 and the introduction of pyrite. With the increase in the F/P mole ratio (Samples C and D), the concentration of Pb and O atoms overall decreased, but the concentration of Fe and S atoms increased. Additionally, the concentration of C atoms fluctuated after the thermochemical treatment, which could be attributed to the introduction of polluting carbon and the residue PbCO_3 .

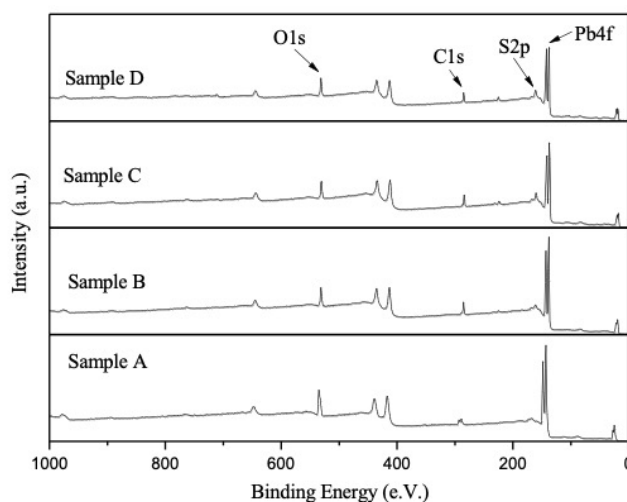


Fig. 6. Full range XPS spectra of the cerussite before and after thermochemical processing with pyrite (Sample A: Raw sample; Samples B-D: F/P mole ratios of 0.1, 0.2 and 0.4)

Table 1. Atomic concentration of elements as determined by XPS

Samples	Atomic concentration (%)				
	Pb4f	Fe2p	O1s	C1s	S2p
A	13.33	0.61	49.64	36.42	0
B	15.24	0.73	34.64	39.80	9.58
C	13.94	2.06	31.62	36.96	15.41
D	12.38	3.69	32.29	37.00	14.65

Fig. 7 shows the high-resolution XPS spectra of Pb4f, S2p, O1s and C1s, and their respective assignments and properties are listed in Tables 2-5. Fig. 7(a) presents the Pb4f spectra of the cerussite before and after thermochemical processing. The Pb4f XPS spectrum of the un-treated cerussite (Sample A) showed a doublet attributed to the $\text{Pb}4f_{7/2}$ and $\text{Pb}4f_{5/2}$ levels. Therefore, both peaks had the same characteristics. The $\text{Pb}4f_{7/2}$ binding energy at 138.86 eV was ascribed to PbCO_3 (Cozza et al., 1992; Feng et al., 2016). The fitting results of the $\text{Pb}4f_{7/2}$ peak in the spectrum of the cerussite after thermochemical processing with an F/P mole ratio of 0.1 (Sample B) indicated that the peak consisted of three components. Combined with Table 2, the peak at a binding energy of 137.32 eV with a proportion of 47.51% was attributed to Pb in the generated PbS (Lara et al., 2011; Mikhlin et al., 2015). The other peak at a binding energy of 138.31 eV with a proportion of 50.79% was attributed to Pb in the generated PbO (Gupta et al., 1996; Kannan et al., 2014). The third peak at a binding energy of 139.58 eV with a proportion of 1.7% was ascribed to the Pb in the generated lead sulfates (Chastain, 1992; Zhou et al., 2014), such as PbSO_4 , $\text{PbO} \cdot \text{PbSO}_4$ and $4\text{PbO} \cdot \text{PbSO}_4$. With the increase in the F/P mole ratios (Samples C and D), the proportion of Pb in the generated PbS and lead sulfates overall increased, but the proportion of Pb in the generated PbO decreased, which corresponds to the changes of the peak intensity in Fig. 7(a). These results were also supported by the XRD (Fig. 4) and thermodynamic analyses (Fig. 5).

The S atomic concentration on the surface of the treated cerussite confirmed that the cerussite was sulfurized by pyrite at a high temperature, as shown in Table 1. However, it could not reveal the chemical state and composition of S in the treated samples. Therefore, the S2p XPS analyses of the cerussite after thermochemical processing needed to be analysed in detail, as shown in Fig. 7(b) and Table 3. Fig. 7(b) presents that the S2p XPS spectrum consisted of a doublet structure of S2p_{3/2} and S2p_{1/2} levels. Although the strength of S2p_{3/2} is greater than that of S2p_{1/2}, the peaks had the same properties. The results of curve fitting of the S2p_{3/2} peak showed three well separated peaks in binding energy ranges of 160.47-160.84 eV, 161.91-162.29 eV and 167.95-168.54 eV. By consulting the available literature on the binding energy of S2p_{3/2} (Smart et al., 1999; Ikumapayi et al., 2012; Feng et al., 2016; Jia et al., 2019; Wang et al., 2019), the components in the abovementioned binding energy ranges could be assigned to the sulfur in the generated PbS (Ikumapayi et al., 2012; Jia et al., 2019), PbS₂ (Smart et al., 1999; Feng et al., 2016) and lead sulfates (Ikumapayi et al., 2012; Wang et al., 2019), such as PbSO₄, PbO·PbSO₄ and 4PbO·PbSO₄. These results further confirmed the results obtained by analysing the Pb4f_{7/2} XPS spectra in Fig. 7(a). According to Table 3, the percentage of S in PbS increased, but the percentage of S in PbS₂ and lead sulfates decreased with the increase in the F/P mole ratios. Generally, more PbS formed on the mineral surface was advantageous to improve the flotation performance. These results further agreed with the increase in the flotation recovery of the cerussite modified with a higher F/P mole ratio (0.4), as shown in Fig. 3.

Figs. 7(c-d) show the high-resolution O1s and C1s XPS spectra of the cerussite before and after thermochemical processing, and Tables 4 and 5 presents both the assignments and properties. In the spectrum of the untreated sample (Sample A), the fitting of the O1s peak, as shown in Fig. 7(c), revealed two components located at 531.03 and 532.49 eV. Combined with Table 4, the peak centred at 531.03 eV with an average proportion of 94.86% was associated with O in PbCO₃ (Feng et al., 2016). The other peak was related to O in the C-O functional group (Nowak and Laajalehto, 2007; Bai et al., 2018). The fitting of the C1s peak, as shown in Fig. 7(d), revealed three components located at 284.76, 285.69 and 289.32 eV. The peak located at 289.32 eV with an average proportion of 45.85% (Table 5) was associa-

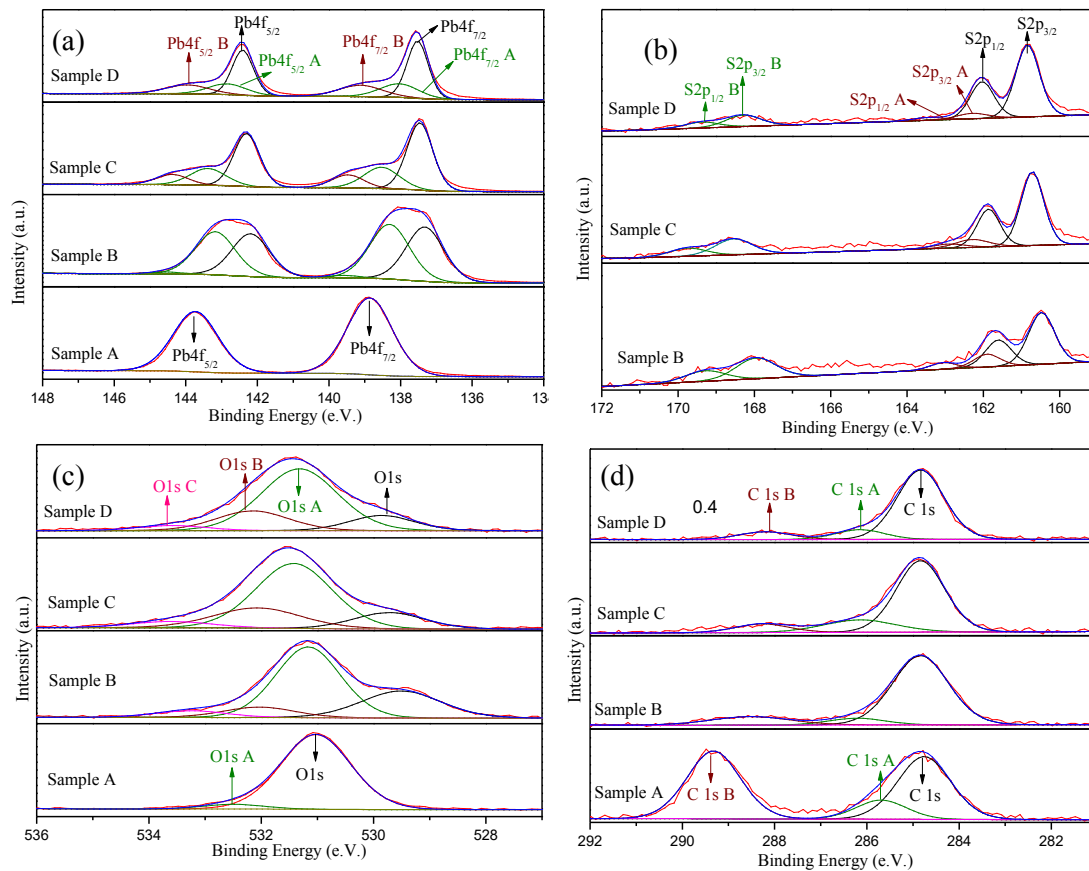


Fig. 7. High-resolution XPS spectrums of Pb4f (a), S2p (b), O1s (c) and C1s (d) (Sample A: Raw sample; Samples B-D: F/P mole ratios of 0.1, 0.2 and 0.4)

ted with C in PbCO_3 (Buckley et al., 2003; Feng et al., 2016), which further agreed with the fitting results of $\text{Pb}4f$ and $\text{O}1s$. The other two peaks located at 284.76 and 285.69 eV were ascribed to carbon contamination in the form of C-H and C-O species (Bai et al., 2018). In the spectra of the cerussite after thermochemical processing (Samples B-D), the fitting of the $\text{O}1s$ peak, as shown in Fig. 7(c), revealed four components in binding energy ranges of 529.51-529.86 eV, 531.17-531.42 eV, 532.03-532.16 eV and 533.25-533.60 eV, which were related to O in the generated PbO (Ikumapayi et al., 2012), sulfates (Chastain, 1992), C-O species (Bai et al., 2018; Nowak and Laajalehto, 2007) and O=C-O functional groups (Nowak et al., 2000), respectively. According to Table 4, the percentage of O in PbO decreased, but the percentage of O in the lead sulfates increased with the increase in the F/P mole ratio, which was consistent with the thermodynamic analyses. The fitting of the $\text{C}1s$ peak, as shown in Fig. 7(d), revealed three components in binding energy ranges of 284.83-284.84 eV, 286.15-286.21 eV and 288.21-288.52 eV. Only the component in the binding energy range of 288.21-288.52 eV was contributed by C in the residue PbCO_3 and even $\text{PbO} \cdot \text{PbCO}_3$ (Buckley et al., 2003; Feng et al., 2016). The other two components were associated with the pollution caused by the functional groups of C-H and C-O (Bai et al., 2018). From Table 5, the percentage of C in the residue PbCO_3 decreased, which further revealed that the introduction of the sulfidation agent facilitated the decomposition of PbCO_3 .

Table 2. Assignment and properties of the $\text{Pb}4f_{7/2}$ XPS

Samples	Binding energy (eV)			Atomic concentration ratio (%)		
	PbS	PbO	Sulfates	PbS	PbO	Sulfates
A	-	138.86	-	-	100.00	-
B	137.32	138.31	139.58	47.51	50.79	1.70
C	137.46	138.53	139.47	59.61	26.11	14.28
D	137.52	138.04	139.11	54.36	23.51	22.13

Table 3. Assignment and properties of the $\text{S}2p_{3/2}$ XPS

Samples	Binding energy (eV)			Atomic concentration ratio (%)		
	PbS	PbS ₂	Sulfates	PbS	PbS ₂	Sulfates
B	160.47	161.91	167.95	53.65	13.26	33.09
C	160.71	162.29	168.54	66.39	10.32	23.29
D	160.84	162.29	168.29	75.22	7.24	17.54

Table 4. Assignment and properties of the $\text{O}1s$ XPS

Samples	Binding energy (eV)				Atomic concentration ratio (%)			
	PbO	Sulfates	C-O	O=C-O	PbO	Sulfates	C-O	O=C-O
A	531.03	-	532.49	-	94.86	-	51.14	-
B	529.51	531.17	532.03	533.25	27.05	57.59	9.35	6.00
C	529.72	531.42	532.07	533.60	13.88	59.01	21.09	6.01
D	529.86	531.32	532.16	533.58	13.10	63.12	19.14	4.65

Table 5. Assignment and properties of the $\text{C}1s$ XPS

Samples	Binding energy (eV)			Atomic concentration ratio (%)		
	C-H	C-O	PbCO_3	C-H	C-O	PbCO_3
A	284.76	285.69	289.32	42.06	12.08	45.85
B	284.84	286.21	288.52	78.57	7.69	13.74
C	284.84	286.15	288.26	71.86	18.56	9.58
D	284.83	286.15	288.21	78.78	11.51	9.70

3.4. EPMA analyses

Fig. 8 shows the EPMA images and EDS line scanning spectra of the cerussite after thermochemical processing with different F/P mole ratios. From Figs. 8 (a-c), there were no obvious changes at the

outlayer of most of the obtained massicot (PbO) particles after thermochemical processing with pyrite at an F/P mole ratio of 0.1. When the F/P mole ratio increased to 0.2, a large number of particles with an obvious layered configuration was formed. With a further increase in the F/P mole ratio, the demarcation line between the massicot and the generated sulfur-bearing mineral nearly disappeared and the layered configuration became more compact.

Figs. 8 (a1-c1) are enlarged views of Figs. 8 (a-c), and their respective EDS line scanning spectra are shown in Figs. 8 (d-f). Overall, the interior of the particles was mainly composed of the massicot and

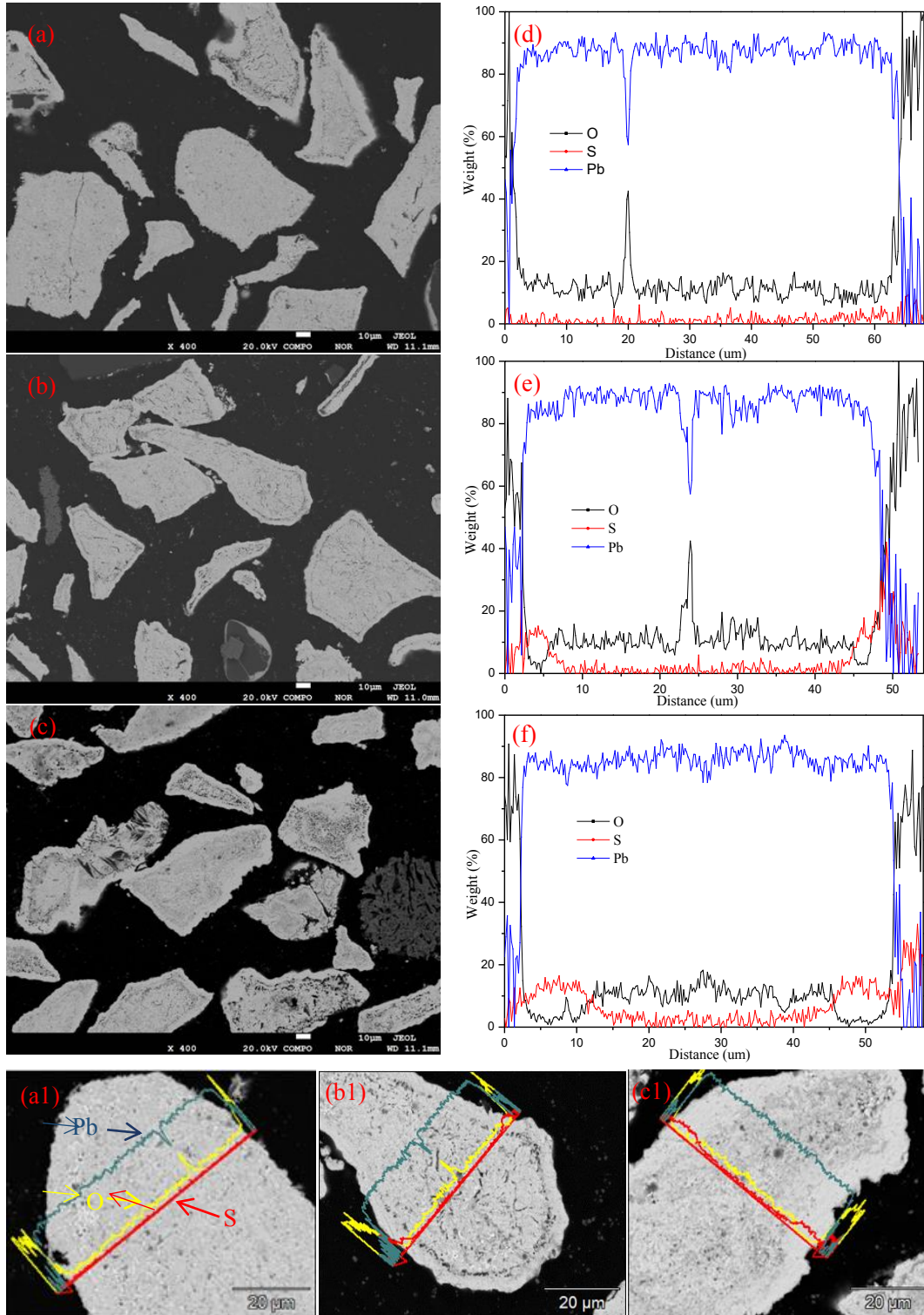


Fig. 8. EPMA images and EDS line scanning spectra of the cerussite after thermochemical processing with pyrite (a, a1 and d: F/P mole ratio of 0.1; b, b1 and e: F/P mole ratio of 0.2; c, c1 and f: F/P mole ratio of 0.4)

the outlayer of the particles was composed of sulfur-bearing compounds, such as lead sulfide (mainly) and sulfates. The sulfur content at an F/P mole ratio of 0.1 (Fig. 8 (d)) slightly fluctuated over the whole section of the particle, and the signal of S presented a straight line in Fig. 8 (a1). When the F/P mole ratio increased to 0.2, the sulfur content at the outer section of the particle increased, corresponding to the intensification of the sulfur signals. With a further increase in the F/P mole ratio, the sulfur content at the outer section of the particle further increased, corresponding to a further intensification of the sulfur signals. In addition, it was observed that the thickness of the generated sulfur-bearing compounds increased with the increase in the F/P mole ratio. The thickness of the products increased to approximately 10 μm at an F/P mole ratio of 0.4, as shown in Fig. 8 (c1). However, the oxygen content at the outer section of the particle decreased, in contrast with the sulfur content, but the lead content showed little change, which revealed that the sulfidation reactions occurred at the surface of the obtained massicot (PbO) to form mainly PbS. Combined with Fig. 3, the recovery of the cerussite after modification with the same mole ratio (0.4) reached approximately 90% under moderate flotation conditions. These results confirmed that modification at only the outer of the cerussite, not complete transformation of the cerussite, can facilitate the flotation of the mineral.

4. Conclusions

The current work systematically investigated the surface modification of cerussite by thermochemical processing with pyrite. Based on the above results and discussions, the following conclusions are reached:

- (1) The cerussite after thermochemical processing with pyrite at a suitable F/P mole ratio showed good floatability, and the flotation recovery increased to approximately 90%. The increase in the F/P mole ratio was conducive to flotation. In addition, increasing the collector dosage and the pH was beneficial to the flotation, but a higher pH was disadvantageous for the flotation.
- (2) The concentration of O and S atoms on the surface of the modified cerussite decreased and increased, respectively, with the increase in the F/P mole ratio. Lead sulfide species including mainly PbS and PbS₂, were formed on the mineral surface, and the percentage of PbS increased with the increase in the F/P mole ratio, which was beneficial for the flotation of the treated cerussite. Other species, including PbSO₄, PbO·PbSO₄ and 4PbO·PbSO₄ were also detected at the mineral surface.
- (3) An obvious layered configuration was formed and became more compact with the increase in the F/P mole ratio. The thickness of the products increased to approximately 10 μm at an F/P mole ratio of 0.4, and this value was below the theoretical F/P mole ratio (0.6) for complete transformation of PbCO₃ into PbS. The sulfur content at the outer of the particle increased, whereas the oxygen content decreased with the increase in the F/P mole ratio.

Acknowledgements

The authors would like to acknowledge the National Natural Science Foundation of China (No. 51964027), the Yunnan Province Applied Basic Research Project (2017FB084) and the Testing and Analysing Funds of Kunming University of Science and Technology (2018T20150055) for financial supports.

References

- BAI, S., LI, C., FU, X., LIU, J., WEN, S., 2018. *Characterization of Zinc Sulfide Species on Smithsonite Surfaces During Sulfidation Processing: Effect of Ammonia Liquor*. J. Ind. Eng. Chem. 61, 19-27.
- BUCKLEY, A., GOH, S., LAMB, R., WOODS, R., 2003. *Interaction of Thiol Collectors with Pre-oxidised Sulfide Minerals*. Int. J. Miner. Process. 72(1-4), 163-174.
- CHASTAIN, J., 1992 *Handbook of X-ray Photoelectron Spectroscopy*. Perkin-Elmer Corporation. 40, 221.
- CHEN, L.Z., WANG, C.B., ZHENG, Y.X., LV, J.F., LAI, Z.N., PANG, J., 2019. *Flotation of A Low-Grade Zinc Oxide Ore After Surface Modification at High Temperature*. JOM. 71(9), 3166-3172.
- COZZA, C., DI CASTRO, V., POLZONETTI, G., MARABINI, A., 1992 *An X-ray Photoelectron Spectroscopy (XPS) Study of the Interaction of Mercapto-benzo-thiazole With Cerussite*. Int. J. Miner. Process. 34(1-2), 23-32.
- FENG, Q., WEN, S., ZHAO, W., DENG, J., XIAN, Y., 2016. *Adsorption of Sulfide Ions on Cerussite Surfaces and Implications for Flotation*. Appl. Surf. Sci. 360, 365-372.

- FUERSTENAU, M., OLIVAS, S., HERRERA-URBINA, R., HAN, K., 1987. *The Surface Characteristics and Flotation Behavior of Anglesite and Cerussite*. Int. J. Miner. Process. 20(1-2), 73-85.
- GOLSHEIKH, A.M., HUANG, N., LIM, H., CHIA, C.H., HARRISON, I., MUHAMAD, M., 2013. *One-pot Hydrothermal Synthesis and Characterization of FeS₂ (pyrite)/graphene Nanocomposite*. Chem. Eng. J. 218, 276-284.
- GUPTA, S.M., KULKARNI, A.R., VEDPATHAK, M., KULKARNI, S.K., 1996. *Surface Study of Lead Magnesium Niobate Ceramic Using X-ray Photoelectron Spectroscopy*. Mater. Sci. Eng. B, 39(1), 34-40.
- GUSH, J., 2005. *Flotation of Oxide Minerals by Sulphidization-the Development of A Sulphidization Control System for Laboratory Testwork*. J. South. Afr. Inst. Min. Metall. 105(3), 193-198.
- HERRERA-URBINA, R., SOTILLO, F., FUERSTENAU, D., 1998. *Amlyl Xanthate Uptake by Natural and Sulfide-treated Cerussite and Galena*. Int. J. Miner. Process. 55(2), 113-128.
- IKUMAPAYI, F., MAKITALO, M., JOHANSSON, B., RAO, K.H., 2012. *Recycling of Process Water in Sulphide Flotation: Effect of Calcium and Sulphate Ions on Flotation of Galena*. Miner. Eng. 39, 77-88.
- IVANOV, I., STEFANOV, Y., NONCHEVA, Z., PETROVA, M., DOBREV, T., MIRKOVA, L., VERMEERSCH, R., DEMAEREL, J.P., 2000. *Insoluble Anodes Used in Hydrometallurgy: Part II. Anodic Behaviour of Lead and Lead-alloy Anodes*. Hydrometallurgy. 57(2), 125-139.
- JIA, Y., HUANG, X., HUANG, K., WANG, S., CAO, Z., ZHONG, H., 2019. *Synthesis, Flotation Performance and Adsorption Mechanism of 3-(ethylamino)-N-phenyl-3-thioxopropanamide onto Galena/sphalerite Surfaces*. J. Ind. Eng. Chem. 77,416-425.
- KANNAN, K., MUTHURAMAN, G., MOON, I.S., 2014. *Controlled Synthesis of Highly Spherical Nano-PbO₂ Particles and Their Characterization*. Mater. Lett. 123, 19-22.
- KORSHIN, G.V., FERGUSON, J.F., LANCASTER, A.N., 2000. *Influence of Natural Organic Matter on the Corrosion of Leaded Brass in Potable Water*. Corros. Sci. 42(1), 53-66.
- LARA, R.H., BRIONES, R., MONROY, M.G., MULLET, M., HUMBERT, B., DOSSOT, M., NAJA, G.M., CRUZ, R., 2011. *Galena Weathering under Simulated Calcareous Soil Conditions*. Sci. Total Environ. 409(19), 3971-3979.
- LI, C.X., WEI, C., SONG, Y., DENG, Z.G., LIAO, J.Q., XU, H.S., LI, M.T., LI, X.B., 2012. *Hydrothermal sulfidation of white lead with elemental sulfur*, Adv. Mater. Res. 396-398, 624-630.
- LI, Y., WANG, J.-K., WEI, C., LIU, C.-X., JIANG, J.-B., WANG, F., 2010. *Sulfidation Roasting of Low Grade Lead-zinc Oxide Ore With Elemental Sulfur*. Miner. Eng. 23(7), 563-566.
- Li, ZH., CHEN, M., HUANG, P.-W., ZHANG, Q.-W., SONG, S.-X., 2017. *Effect of Grinding with Sulfur on Surface Properties and Floatability of Three Nonferrous Metal Oxides*. Trans. Nonferrous Met. Soc. China. 27(11), 2474-2480.
- LIANG, Y.J., CHAI, L.Y., LIU, H., MIN, X.B., MAHMOOD, Q., ZHANG, H.-J., KE, Y., 2012. *Hydrothermal Sulfidation of Zinc-containing Neutralization Sludge for Zinc Recovery and Stabilization*. Miner. Eng. 25(1), 14-19.
- LV, W., YU, D., WU, J., ZHANG, L., XU, M., 2015. *The Chemical Role of CO₂ in Pyrite Thermal Decomposition*. Proc. Combust. Inst. 35(3), 3637-3644.
- MALGHAN, S., 1986. *Role of Sodium Sulfide in the Flotation of Oxidized Copper, Lead, and Zinc Ores*. Min., Metall., Explor. 3(3), 158-163.
- MAY, G.J., DAVIDSON, A., MONAHOV, B., 2018. *Lead Batteries for Utility Energy Storage: A Review*. J. Energy Storage. 15, 145-157.
- MIKHLIN, Y.L., KARACHAROV, A.A., LIKHATSKI, M.N., 2015. *Effect of Adsorption of Butyl Xanthate on Galena, PbS, and HOPG Surfaces as Studied by Atomic Force Microscopy and Spectroscopy and XPS*. Int. J. Miner. Process. 144, 81-89.
- NOWAK, P., LAAJALEHTO, K., 2007. *On the Interpretation of the XPS Spectra of Adsorbed Layers of Flotation Collectors-ethyl Xanthate on Metallic Lead*. Physicochem. Probl. Miner. Process. 41, 107-116.
- NOWAK, P., LAAJALEHTO, K., KARTIO, I., 2000. *A Flotation Related X-ray Photoelectron Spectroscopy Study of the Oxidation of Galena Surface*. Colloids Surf., A. 161(3), 447-460.
- POWELL, K.J., BROWN, P.L., BYRNE, R.H., GAJDA, T., HEFTER, G., LEUZ, A.-K., SJOBERG, S., WANNER, H., 2013. *Chemical Speciation of Environmentally Significant Metals with Inorganic Ligands. Part 5: The Zn²⁺, OH⁻, Cl⁻, CO₃²⁻, SO₄²⁻, and PO₄³⁻-Systems (IUPAC Technical Report)*. Pure Appl. Chem. 85(12), 2249-2311.
- ROINE, A., 2002. *Outokumpu HSC chemistry for windows: Chemical Reaction and Equilibrium Software with Extensive Thermochemical Database*. Pori: Outokumpu research OY.
- SHARONOV, M.Y., BYKOV, A., PETRICEVIC, V., ALFANO, R., 2008. *Spectroscopic Study of Optical Centers Formed in Bi-, Pb-, Sb-, Sn-, Te- and In-doped Germanate Glasses*. Opt. Lett. 33(18), 2131-2133.
- SHIROTA, Y., NIKI, K., SHINDO, H., 2011. *Stabilities of Crystal Faces of Aragonite-type Strontianite (SrCO₃) and Cerussite (PbCO₃) Compared by AFM Observation of Facet Formation in Acid*. J. Cryst. Growth. 324(1), 190-195.

- SMART, R.S.C., SKINNER, W.M., GERSON, A.R., 1999. XPS of Sulphide Mineral Surfaces: Metal-deficient, Polysulphides, Defects and Elemental Sulphur. *Surf. Interface Anal.* 28(1), 101-105.
- TANG, Y.-Y., BI, X.-W., FAYEK, M., HU, R.-Z., WU, L.-Y., ZOU, Z.-C., FENG, C.-X., WANG, X.-S., 2014. Microscale Sulfur Isotopic Compositions of Sulfide Minerals from the Jinding Zn–Pb Deposit, Yunnan Province, Southwest China. *Gondwana Research.* 26(2), 594-607.
- WANG, C., DENG, J., CARRANZA, E.J.M., LAI, X., 2014. Nature, Diversity and Temporal–spatial Distributions of Sediment-hosted Pb–Zn deposits in China. *Ore Geol. Rev.* 56, 327-351.
- WANG, X., QIN, W., JIAO, F., LIU, R., WANG, D., 2019. Inhibition of Galena Flotation by Humic Acid: Identification of the Adsorption Site for Humic Acid on Moderately Oxidized Galena Surface. *Miner. Eng.* 137, 102-107.
- YUAN, W., LI, J., ZHANG, Q., SAITO, F., 2012. Mechanochemical Sulfidization of Lead Oxides by Grinding with Sulfur. *Powder Technol.* 230, 63-66.
- ZHENG, Y.X., LIU, W., QIN, W.Q., JIAO, F., HAN, J.W., YANG, K., LUO, H.L., 2015. Sulfidation Roasting of Lead and Zinc Carbonate with Sulphur by Temperature Gradient Method. *J. Cent. South Univ.* 22(5), 1635-1642.
- ZHENG, Y.X., LV, J.F., WANG, H., WEN, S.M., HUANG, L., 2018a. Efficient sulfidization of lead oxide at high temperature using pyrite as vulcanizing reagent. *Physicochem. Probl. Miner. Process.* 54(2), 270-277.
- ZHENG, Y.X., LV, J.F., WANG, H., WEN, S.M., PANG, J., 2018b. Formation of zinc sulfide species during roasting of ZnO with pyrite and its contribution on flotation. *Sci. Rep.* 8(1), 7839.
- ZHOU, J., ZHAO, H., SHI, J., CHEN, Q., SHEN, X., 2014. Radiolytic Synthesis of Prismatic PbSO₄ Microcrystals. *Radiat. Phys. Chem.* 97, 366-369.